

Reducing uncertainty in geologic CO₂ sequestration risk assessment by assimilating monitoring data

Bailian Chen*, Dylan R. Harp, Zhiming Lu, Rajesh J. Pawar

Earth and Environmental Sciences Division, Los Alamos National Laboratory, Los Alamos, NM 87544, USA



ARTICLE INFO

Keywords:

Geologic CO₂ sequestration
Risk assessment
Conditional simulation
Data assimilation
Uncertainty reduction analysis

ABSTRACT

Geologic CO₂ sequestration sites usually have large uncertainty in geological properties, such as uncertainty in permeability and porosity fields. Geological uncertainty leads to significant uncertainty in predicted risk metrics such as CO₂ plume extent, CO₂/brine leakage rates through wellbores, and impacts to drinking water quality in groundwater aquifers due to CO₂/brine leakage, all of which will impact the approach for post injection site care (PISC). Pre-injection risk assessment can be used to quantify the amount of uncertainty in different predicted risk metrics. However, it cannot account for the potential value of monitoring data (e.g., CO₂ saturation and pressure measurements) acquired during the operation of CO₂ storage. In this study, we demonstrate how uncertainty in predicted risks can be reduced by performing monitoring data assimilation. An ensemble of geological reservoir models, constrained by direct measurements (such as permeability estimates from exploratory wells), are generated by geostatistical conditional simulation. As the monitoring data from the storage site become available, they are assimilated into models using a recently developed data assimilation method, ES-MDA with geometric inflation factors (ES-MDA-GEO). The reservoir models, calibrated through multiple data assimilation iterations, are used to predict future risks and reduction in their uncertainties. The proposed approach for the quantification of uncertainty reduction in risk assessment is demonstrated with two examples: a generalized 3D synthetic case and a synthetic field case based on the Rock Springs Uplift site in southwestern Wyoming.

1. Introduction

Geologic CO₂ sequestration (GCS) is being considered as a strategy to reduce anthropogenic CO₂ emissions (Metz, 2005; Michael et al., 2010). Different types of reservoirs or formations have been proposed to store CO₂ emissions, such as oil or gas reservoirs, coal seams, deep oceans and saline aquifers (Harp et al., 2017; Jin et al., 2017; Liu and Mostaghimi, 2017; Cui et al., 2018; Dai et al., 2018; Chen and Pawar, 2019; Ren and Duncan, 2019; Zhang et al., 2019a, b). A primary concern with GCS projects is the potential for CO₂ and brine leakage risks to overlying resources (e.g., potable groundwater, oil and gas reservoirs, etc.) (Benson and Myer, 2003; Wilkin and DiGiulio, 2010; Harp et al., 2016). To build confidence in GCS, a scientifically-sound quantitative approach for risk management is required to provide reliable predictions (forecasts) of long-term safety and risks of CO₂ storage systems (Condor et al., 2011; De Lary et al., 2015; Li and Liu, 2016). A number of studies demonstrate application of quantitative approaches for risk assessment (Zhang et al., 2011; Nicot et al., 2013; Dai et al., 2014; Pawar et al., 2016; Onishi et al., 2019).

At any GCS site the pre-injection risk assessment is based on the

available site characterization data which may be limited depending on the type of site and level of characterization effort. For example, typically saline aquifers do not have the benefit of prior characterization efforts such as depleted oil/gas reservoirs. The quality and quantity of characterization data will lead to certain level of uncertainty in site predictions including predicted long-term risks. During the injection phase monitoring data, such as pressure and CO₂ saturation measurements, are usually collected from monitoring wells. As more monitoring data become available, it can be used to update and refine predictive models leading to better representation of the system and potentially less uncertainty in model outputs and improved predictions. Effectively incorporating new monitoring data throughout the GCS operation requires a formal strategy that can efficiently assimilate the data, update model parameters (or indicate model modifications if necessary), quantify the resulting uncertainty (potentially reducing the uncertainty and narrowing of uncertainty bands around outputs of interest), and ultimately provide implications for the reduction in risk associated with the GCS operation. In this study, we demonstrate how the uncertainty in predicted risk metrics changes with assimilation of monitoring data. Our approach includes sequentially conducting geostatistical

* Corresponding author.

E-mail address: bailianchen@lanl.gov (B. Chen).

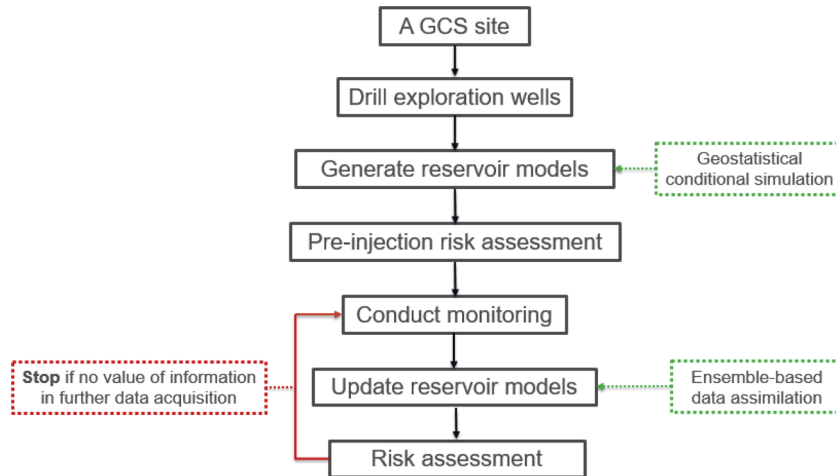


Fig. 1. The proposed workflow for geologic CO₂ sequestration risk assessment.

conditional simulation for generating reservoir models and ensemble-based data assimilation. To the best of our knowledge, uncertainty reduction analyses in risk assessment are currently scarce in existing literature. Next, we provide a discussion of some of the most relevant work on data assimilation and uncertainty quantification in order to put the methodology introduced in this paper in the proper context.

Oladyshev et al. (2013) proposed a framework based on polynomial chaos expansion (PCE) and bootstrap filtering for assimilating pressure data into reservoir models and quantify the uncertainty reduction in CO₂ leakage rate at a storage site. They considered three uncertain parameters: reservoir permeability, reservoir porosity and wellbore permeability. Chen et al. (2018) demonstrated an approach based on a machine learning technique and a filter-based data assimilation method to perform CO₂ monitoring design. In this approach, the optimal monitoring design can be determined based on choosing a design that reduces the uncertainty in the predictions of cumulative CO₂ leakage. Though the methods for data assimilation proposed by Oladyshev et al. and Chen et al. are computationally efficient, their methods are limited to cases where only a limited number of uncertain parameters are involved. Jia et al. (2018) proposed an approach based on Bayesian model averaging and Monte Carlo simulations to quantify the uncertainty at a site in western Texas. In their work, Monte Carlo simulations were conducted to quantify parameter uncertainty due to heterogeneity in porosity and permeability. Monte Carlo simulations were conducted via reduced order models which were developed using a PCE method. Then, the Bayesian model averaging method was used to quantify model uncertainty. Sun and Durlofsky (2019) developed a data-space inversion (DSI) approach to quantify uncertainty of CO₂ plume locations during GCS. In the DSI approach, posterior predictions (forecast) of CO₂ saturation distribution are generated using simulation results for prior model realizations along with observed data. Note that posterior geological models are not generated in the DSI method, which is different from the traditional data assimilation method such as ensemble-based data assimilation approaches.

In the last decade, ensemble-based methods have been widely used for data assimilation of sub-surface flow problems in both hydrologic applications and the petroleum industry. Among the ensemble-based methods, the ensemble Kalman filter (EnKF) is the most popular for data assimilation (or history-matching) applications (Aanonsen et al., 2009; Evensen, 2009; Chang et al., 2010; Chen and Oliver, 2010). Emerick and Reynolds (2013) proposed a new data assimilation approach, i.e., Ensemble Smoother with Multiple Data Assimilation (ES-MDA) and demonstrated the superiority of ES-MDA over EnKF for data assimilation. The main drawback of ES-MDA is that the total number of data assimilation steps and the inflation factors for each assimilation iteration must be specified before starting data assimilation processes.

Recently, a more practical and efficient version of this approach called ES-MDA with geometric inflation factors (ES-MDA-GEO) was proposed by Rafiee and Reynolds (2017). This method allows the user to specify a priori the total number of data assimilation steps which is determined based on the allowable computational resources, while at the same time providing sufficient damping of changes in the reservoir model realizations. This recently developed algorithm, ES-MDA-GEO, is implemented in this study for assimilating monitoring data collected during GCS projects.

This paper is organized as follows: we first present the methodology for this work, including the risk assessment workflow, the geostatistical conditional simulation method, and the ES-MDA-GEO method for data assimilation and uncertainty reduction analysis. Then, the proposed method for risk assessment based on data assimilation and uncertainty reduction analysis is demonstrated with two examples: a 3D synthetic case and a synthetic field case based on the Rock Springs Uplift site in southwestern Wyoming. Finally, we summarize the results and present the conclusions of the paper.

2. Methodology

2.1. Workflow for risk assessment

A workflow for predicting risks and updating predictions with monitoring data at a GCS site is shown in Fig. 1. For a given GCS site, a few exploratory wells will be drilled to characterize the site including properties (e.g., permeability, porosity and rock compressibility) of the target reservoir. These data are subsequently used to develop geologic and reservoir models. Various approaches can be used for developing the models and using them for predictions and uncertainties associated with predictions. One approach is to use stochastic approaches such as geostatistical conditional simulations to generate an ensemble of realizations of heterogeneous reservoir properties. These ensemble models can be used to perform pre-injection risk assessment to quantify the preliminary uncertainties associated with different quantities, such as the predictions (forecasts) of CO₂ saturation/pressure at monitoring or legacy wells, CO₂ saturation/pressure plume area, plume mobility/spreading, as well as risk metrics such as CO₂/brine leakage rates through wellbores, etc. There are uncertainties associated with these predicted quantities depending on the uncertainty in the characterization data. Once CO₂ injection begins, it results in monitoring data. Monitoring data can be used to update and refine predictive models and reduce the uncertainty in predictions. Assimilation of monitoring data can be done using an ensemble-based method such as ES-MDA-GEO. We use a synthetic site to demonstrate the monitoring data assimilation approach using ensemble-based method and its effect on uncertainty

reduction. Next, we provide more details on geostatistical conditional simulations for generating multiple, equi-probable spatial distributions of geologic properties, data assimilation and uncertainty reduction analysis.

2.2. Geostatistical conditional simulation

Geostatistical conditional simulation is widely used in hydrology and petroleum engineering to characterize heterogeneity in reservoirs (PetroWiki, 2012). Conditional simulation preserves not only the statistics of the observed data (e.g., mean and variance) and their spatial correlation but also honors specific observations such as data measured at characterization wells. The stochastic property of conditional simulation allows generation of many equally probable geological realizations which can be used to quantify uncertainty in predictions.

In GCS, direct measurements such as permeability estimates from characterization wells at a storage site are generally expected to be available. These direct measurements can be used as the inputs for conditional simulation to populate permeability fields in reservoir models for numerical simulation. In this study, the GSLIB Software (Deutsch and Journel, 1998) is employed to perform conditional simulation where the measurements of permeability at characterization wells are honored into models when generating heterogeneous reservoir models. To perform ensemble-based data assimilation using ES-MDA-GEO (which will be discussed in detail next) and quantify uncertainty effectively, 100 permeability fields are generated using GSLIB. These permeability fields are used to generate reservoir models for performing pre-injection reservoir performance predictions using LANL's FEHM simulator [34] and subsequent predictions of a few risk metrics. These models are called "prior models" in subsequent sections.

2.3. Data assimilation using ES-MDA-GEO

To generate estimates of the ground truth model and to quantify the uncertainty reduction in the risk assessment, there generally can be an infinite number of reservoir models that are consistent with observations (i.e., monitoring data) in the probabilistic context. Ensemble-based data assimilation methods such as Ensemble Smoother with Multiple Data Assimilation (ES-MDA) can be easily embedded in this probabilistic framework. ES-MDA was first proposed by Emerick and Reynolds (2013), who demonstrated that ES-MDA is superior over EnKF for data assimilation. Though ES-MDA has been demonstrated to be a promising method for assimilating data in sub-surface flow problems (Silva et al., 2017; Evensen, 2018; Kim et al., 2018), the main disadvantage of ES-MDA is that the total number of data assimilation steps and the inflation factors for each assimilation step must be specified before starting data assimilation or history matching processes. To address these issues with the application of ES-MDA, Le et al. (2016) proposed an adaptive ES-MDA method in which the inflation factors are updated at each assimilation step. Although this has improved the performance of the original ES-MDA, it often requires a large number of assimilation steps which may be computationally infeasible for large-scale field examples. Recently, Rafiee and Reynolds (2017) proposed a practical and efficient method to determine the exact minimum inflation factor at each data assimilation step. This method allows the user to specify *a priori* the total number of data assimilation steps which is determined based on the allowable computational resources, while at the meantime providing sufficient damping of changes in the reservoir model realizations at each iteration to control overshooting and undershooting that can cause rough or inaccurate estimates of reservoir models. This new proposed ES-MDA algorithm is called ES-MDA-GEO and is implemented in this study for assimilating monitoring data collected during GCS projects. The following is the pseudo-code for the implementation of conditional simulation and data assimilation.

Pseudo-code for the implementation of conditional simulation and data assimilation:

```

1. Generate initial ensemble models denoted by  $\{m_j^{a,0}\}_{j=1}^{N_e}$  using geostatistical conditional simulation.
2. Choose the number of data assimilation steps,  $N_a$ .
3. For  $i = 1$  to  $N_a$ :
   ◇ Set  $m_j^{f,i} = m_j^{a,i-1}$  for  $j = 1, 2, \dots, N_e$ .
   ◇ Run the ensemble models from time zero.
   ◇ Calculate  $\Delta M^i$  and  $\Delta D^i$  using Eqs. 1 and 2, respectively.
   ◇ Calculate  $G_D^i$  using  $G_D^i = C_D^{-1/2} \Delta D^i$ .
   ◇ If ( $i = 1$ ) then
      • Set  $\alpha_1 = \max\{\bar{\lambda}^2, N_a\}$ , where  $\bar{\lambda}$  is average singular value of  $G_D^i$ .
      • Solve  $\frac{1-(1/\beta)^{N_a-1}}{1-(1/\beta)} = \alpha_1$  for  $\beta$ .
   Else
      • Set  $\alpha_i = \beta^{i-1} \alpha_1$ .
   End If
   ◇ For  $j = 1$  to  $N_e$ 
      • For each ensemble number, perturb the observation vector using  $d_{uc,j}^i = d_{obs} + \sqrt{\alpha_i} C_D^{1/2} z_j$ , where  $z_j \sim \mathcal{N}(0, I_{N_d})$ .
      • Update the ensemble using the following equation  $m_j^{a,i} = m_j^{f,i} + \Delta M^i (G_D^i)^T [G_D^i (G_D^i)^T + \alpha_i I_{N_d}]^{-1} C_D^{-1/2} (d_{uc,j}^i - d_j^{f,i})$ .
   End For
End For

```

where m denotes the vector of model parameters; superscripts a and f denote analysis and forecast, respectively; N_e refers to the total number of model realizations; N_a denotes the predefined number of data assimilation steps; ΔM^i and ΔD^i denote the model square root matrix and data square root matrix, respectively, and are defined as

$$\Delta M^i = \frac{1}{\sqrt{N_e - 1}} [m_1^{f,i} - \bar{m}^{f,i}, \dots, m_{N_e}^{f,i} - \bar{m}^{f,i}] \quad (1)$$

$$\Delta D^i = \frac{1}{\sqrt{N_e - 1}} [d_1^{f,i} - \bar{d}^{f,i}, \dots, d_{N_e}^{f,i} - \bar{d}^{f,i}] \quad (2)$$

where

$$\bar{m}^{f,i} = \frac{1}{N_e} \sum_{j=1}^{N_e} m_j^{f,i} \quad (3)$$

$$\bar{d}^{f,i} = \frac{1}{N_e} \sum_{j=1}^{N_e} d_j^{f,i}, \quad (4)$$

G_D^i is the dimensionless sensitivity matrix; C_D is the covariance matrix of observed data measurement errors; α_i is the measurement error inflation factor at the i th data assimilation step; d_{obs} is the vector of observed data; $d_{uc,j}^i$ is a sample from the normal distribution $\mathcal{N}(d_{obs}, \alpha_i C_D)$; $d_j^{f,i}$ denotes the forecast data obtained from the forward model evaluated at $m_j^{f,i}$. Refer to Rafiee and Reynolds (2017) for more details on the theoretical derivation and the implementation of the ES-MDA-GEO algorithm. In this study, the total number of model realizations N_e is 100 and the number of data assimilation steps N_a is 4. Note N_e and N_a are two important input parameters for the ES-MDA-GEO algorithm (refer to the pseudo-code above). The choices for N_e and N_a are based on the recommendation in the works of Emerick and Reynolds (2013); Le et al. (2016) and Rafiee and Reynolds (2017). It is important to note that step 3 in the pseudo-code is repeated if more monitoring data are available from a storage site until it is determined that the value of information (VOI) will not increase with further data acquisition. Here, VOI, defined by the amount of uncertainty reduction in risk quantities, will be introduced next.

2.4. Uncertainty reduction analysis

Uncertainty reduction analysis, one of the key elements in risk assessment, is conducted after the data assimilation process is completed. In this study, we investigated uncertainty reduction in multiple metrics including, predictions (forecasts) of CO₂ saturation and pressure data at monitoring or legacy wells, CO₂ saturation and pressure plume area, and CO₂ saturation/pressure plume mobility and spreading. Various other metrics can also be investigated including, rates of CO₂/brine leakage through wellbores and groundwater aquifer impact (e.g., pH and total dissolved solid (TDS)), but the evaluation of these metrics using a similar analysis approach as the

evaluation of the quantities to be investigated in this study will require quantification of these metrics using the reservoir predictions such as U.S. National Risk Assessment Partnership's (NRAP's) integrated assessment model (IAM) that couples the reservoir model, wellbore model and aquifer model (Pawar et al., 2016), which is out of the scope of this study.

The prior probability density function (PDF) of a metric of interest, J , is denoted as $P(J)$. Note that $P(J)$ is computed based on the prior reservoir models that are generated by using conditional simulation. We denote the amount of uncertainty in a distribution $P(J)$ as $U(P(J))$, which, as in Le and Reynolds (2014), is defined by

$$U(P(J)) = P_{90}(P(J)) - P_{10}(P(J)) \quad (5)$$

where $P_{90}(P(J))$ and $P_{10}(P(J))$ are the 90th and 10th percentiles, respectively, of the distribution $P(J)$. The posterior PDF of J denoted by $P(J|d_{obs})$ can be calculated after the data assimilation process is completed, where $P(J|d_{obs})$ is the probability that the objective J conditional to monitoring data d_{obs} . Here, the uncertainty reduction, U_R , due to monitoring data assimilation, is defined as the difference between the prior uncertainty and the posterior uncertainty in the model output of interest, which is given by

$$U_R = U(P(J)) - U(P(J|d_{obs})) \quad (6)$$

In the uncertainty reduction analysis, the amount of uncertainty reduction in each quantity of interest will be quantified based on Eq. (6). By analyzing the uncertainty reduction in all the quantities that are of interest we can get reasonable understanding of when to stop monitoring at a specific monitoring well.

3. Example 1: 3D synthetic case

3.1. Model description

We use a synthetic model to apply the workflow discussed in the previous section. As a first step, we generate a synthetic "ground truth" field representation. The synthetic model is 4 km in the horizontal direction, 100 m thick and is at 1 km depth from the ground surface. The model has $51 \times 51 \times 11$ nodes in the x, y and z directions respectively. Fig. 2 presents the horizontal log-permeability ($\ln k$) distribution for the top layer for the true reservoir model (i.e., synthetic ground truth). For simplicity, we assume that the other 9 layers have the same permeability distribution as the top layer.

Next we collect permeability values at 5 locations in the field assuming they were collected by drilling exploratory (characterization)

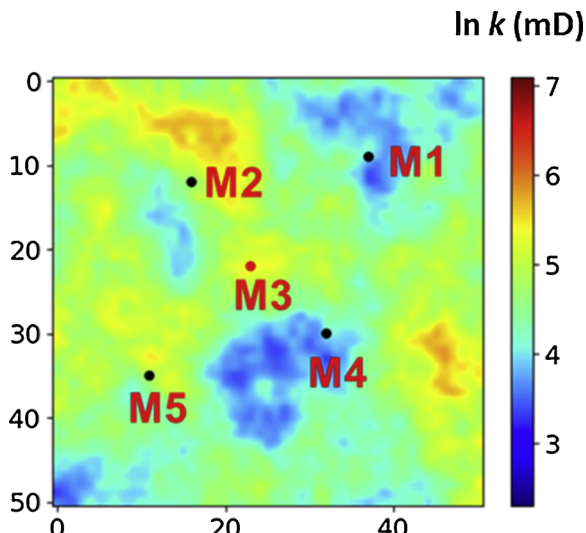


Fig. 2. Log-permeability distribution for the ground truth model and the locations for exploratory wells (M1 through M5).

wells (M1, M2..., and M5) at locations shown in Fig. 2. For our model the reservoir permeabilities at the five exploratory wells, respectively, are 49.75, 92.77, 208.80, 61.02 and 108.51 mD. It is assumed that this is the only characterization information available for generating spatial permeability distributions. The geostatistical conditional simulation will be conducted honoring these direct measurements from exploratory wells to generate the prior reservoir models. Next, we assume that CO₂ is injected at a rate 1 MM tons/year through an injector located at location M3 while the other four wells (M1, M2, M4 & M5) are used as monitoring wells. Note that the locations of monitoring (characterization) wells are randomly chosen, and they are assumed to be the optimal monitoring locations. In previous work, Chen et al. (2018) conducted monitoring design based on machine learning and uncertainty quantification methods to determine the optimal monitoring strategy, i.e., where are the optimal locations to place the monitoring wells(s) and what type of data (pressure, temperature, CO₂ saturation, etc.) should be measured. The focus of this study is to investigate how monitoring data can be used to reduce the uncertainty of risk quantities in geologic CO₂ sequestration; therefore the optimization of monitoring well location is not considered in this study.

We consider a 5-year injection period and 10-year post-injection period. The types of monitoring data collected from the field are pressure and CO₂ saturation. The frequency of data acquisition is once per month, which results in 12 measurements per year for both pressure and CO₂ saturation. If 3 years of monitoring data are collected, then $12 \times 3 \times 2 = 72$ data points will be used to construct the observed data vector, d_{obs} . In addition to the monitoring wells, we collect monitoring data at the injector as well. Since we use a synthetic reservoir, the actual monitoring data are not available. We generate the monitoring data by performing a forward simulation using the "ground truth" model. These monitoring data will be assimilated into the prior reservoir models to update the models and the resulting reduction in prediction uncertainty quantified. The numerical meshes for the reservoir simulation model are generated using the LaGriT grid generation toolkit (<http://lagrit.lanl.gov>) (George et al., 1999). All the required simulations are performed by the FEHM simulator (Zyvoloski et al., 1997).

3.2. Results and analysis

3.2.1. Permeability fields based on conditional simulation

To perform geostatistical conditional simulation and generate pre-injection permeability distributions, we first compute the mean and variance values of the five permeabilities measured at the exploratory (monitoring) wells. Since five permeability values are not enough to evaluate the correlation length of reservoir permeability distribution, we assume the reservoir permeability is isotropic and are spatially correlated with a correlation length of 400 m (corresponding to the five grid block lengths). We use the permeability values at the exploratory wells, the values for mean and variance of permeability distribution, and the assumed correlation length, to generate 100 prior (pre-injection) reservoir permeability distributions using geostatistical conditional simulations. Fig. 3 shows the log-permeability fields generated using the conditional simulation. Only three out of 100 permeability realizations are presented in Fig. 3. It can be seen from Fig. 3 that the permeabilities at the five exploratory wells are honored during conditional simulation, and therefore influence the surrounding permeability values. Comparing with the permeability distribution in the "ground truth" model it can be seen that the permeability distribution of each realization generated from conditional simulation is significantly different indicating large uncertainty in the geostatistically generated distributions.

3.2.2. Model improvement/refinement

It is inevitable to have large uncertainty in pre-injection (prior) geologic and reservoir models when using limited prior information from a storage site. However, the geological uncertainty in the prior models can be reduced by assimilating monitoring data into the models. Fig. 4 shows the permeability distributions of the reservoir models at different stages of data assimilation for one of the 100 realizations. It

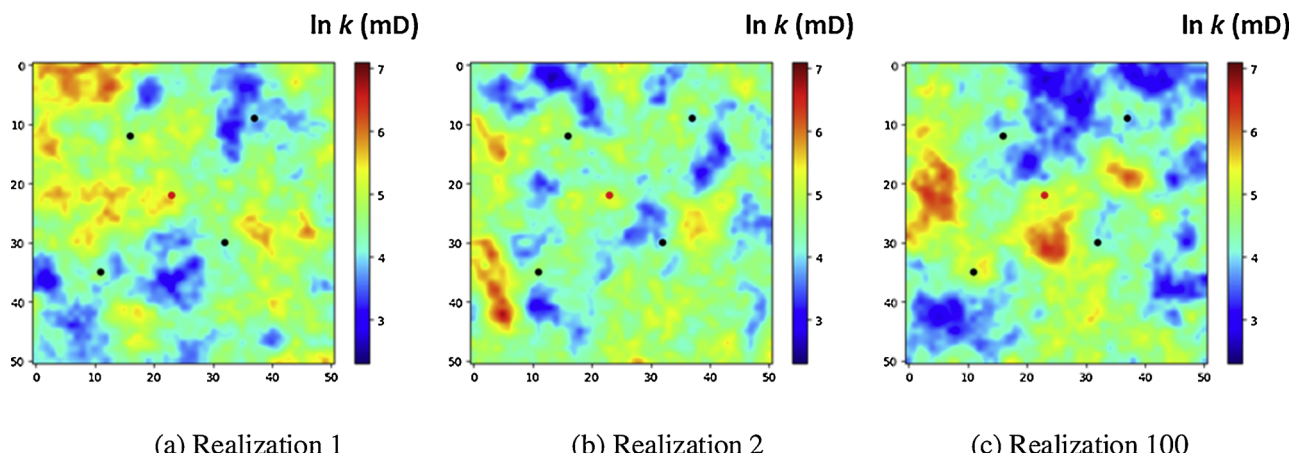


Fig. 3. Log-permeability distributions generated based on conditional simulation.

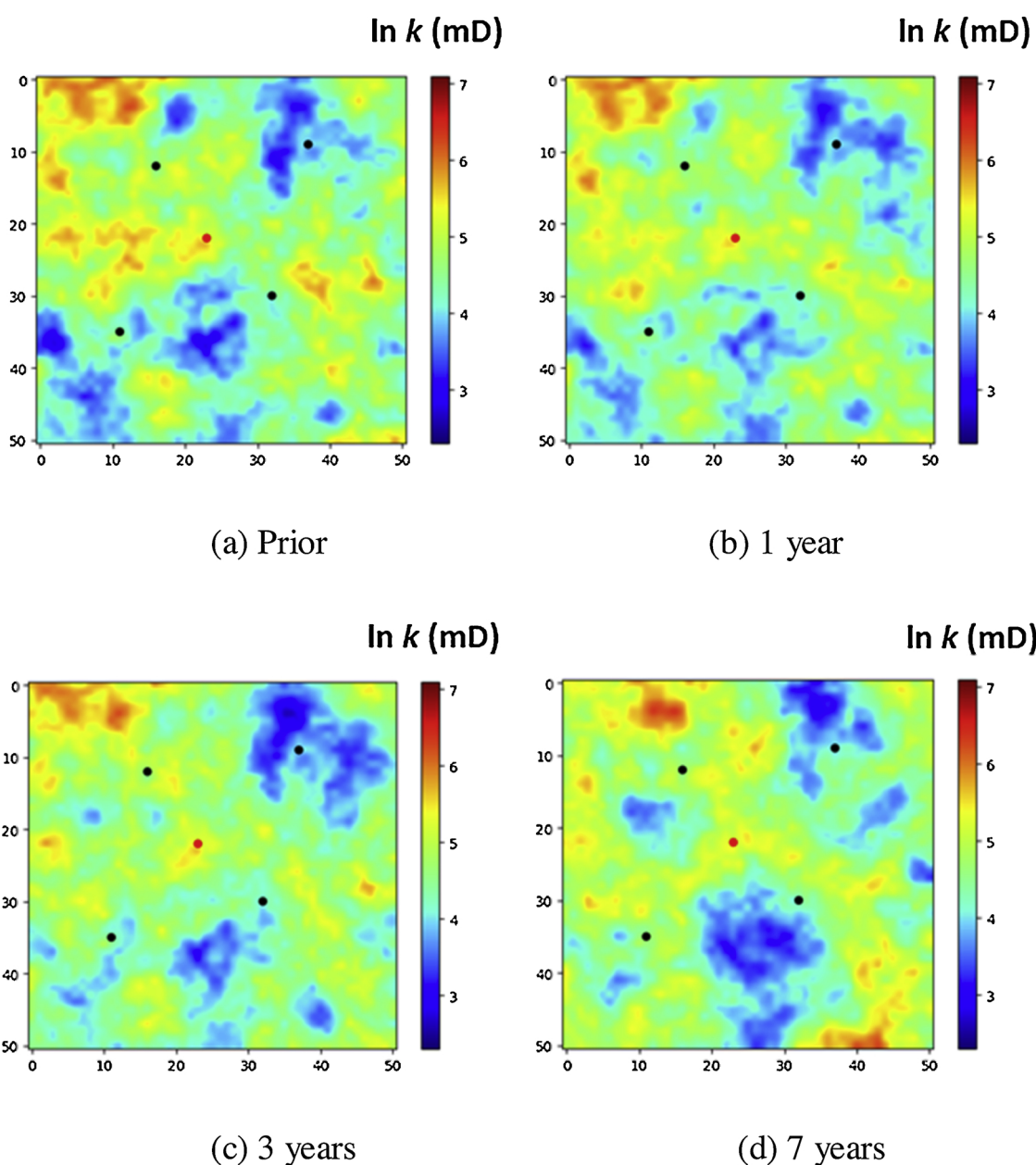


Fig. 4. Model improvement over monitoring time, realization 1, example 1.

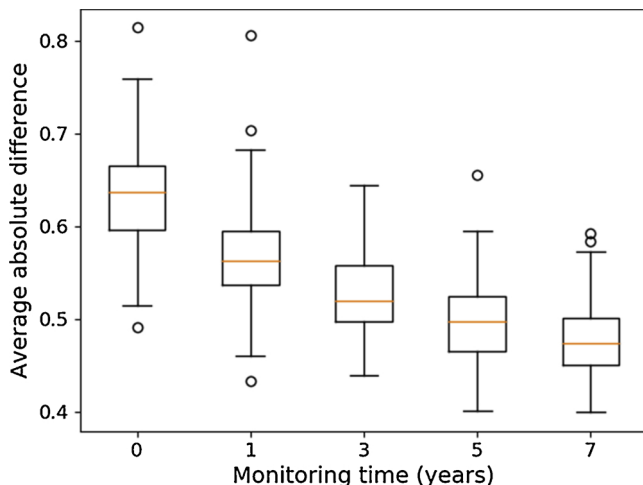


Fig. 5. Boxplot of average absolute difference between calibrated models and the ground truth model over monitoring duration, example 1. Circles in the plot are the outliers; five horizontal lines from bottom to top in each boxplot, respectively, represent the minimum, the 1st quartile, the median, the 3rd quartile and the maximum of a distribution.

can be seen from Fig. 4 that the permeability distribution is getting closer to the “ground truth” model as the monitoring duration increases. This increased similarity between the updated model and the “ground truth” model after assimilation of 7 years monitoring data is apparent. Similar observations were found for other model realizations.

The update/refinement in the permeability fields over the monitoring duration is quantified in Fig. 5. In this figure, the “average absolute difference (AAD)” (y-axis) is defined by the summation of the absolute difference between the log-permeability of an individual node in the updated model and the value of the corresponding node in the “ground truth” model divided by the total number of nodes. A smaller AAD indicates higher similarity between the updated model and the ground truth model. Each boxplot in Fig. 5 is based on 100 AAD values (recall that we have 100 realizations for model updating). We can easily see from this figure that the reservoir models are significantly improved/refined with repeated assimilation of monitoring data.

The effect of the number of monitoring wells on model refinement is investigated by sequentially eliminating monitoring wells M1, M5 and M2 in the field. Fig. 6 shows the boxplot of AAD between calibrated models and the ground truth model by varying the number of monitoring wells. In this Fig. 4 monitoring wells correspond to our original scenario; ‘3’ monitoring wells indicate that monitoring well M1 is eliminated from the analysis; ‘2’ indicates that only M2 and M4 are included; and ‘1’ indicates that only M4 is included. As can be seen from Fig. 6, when more monitoring wells are placed in the field, the reservoir models can be more significantly improved (smaller AAD value) by assimilating the monitoring data. Thus, the extent of model improvement is dependent on the number of monitoring wells. The marginal improvement in AAD is fairly consistent from 1 to 4 monitoring wells. It is not surprising that more wells lead to a better model calibration. However, it is important to note that for a deep saline GCS project, there won’t be too many characterization/monitoring wells (usually less than 5 wells).

3.2.3. Uncertainty reduction analysis over monitoring durations

In this subsection, the uncertainty reduction in the predictions of CO₂ saturation and pressure is discussed. Based on prior reservoir models, we first computed the predictions (forecasts) of CO₂ saturation and pressure at monitoring well locations; shown in Fig. 7. Note that each cyan line corresponds to one prediction of CO₂ saturation or pressure based on one prior model (there are 100 prior models in total). It can be observed that large uncertainties are involved in the

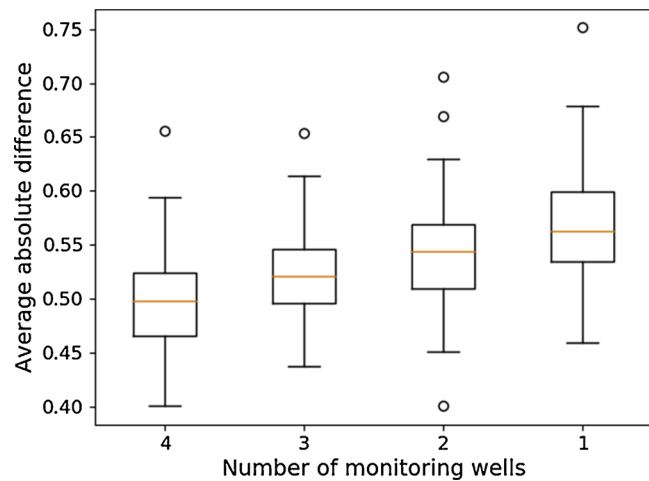


Fig. 6. Boxplot of average absolute difference between calibrated models and the ground truth model by varying the number of monitoring wells; 5-year monitoring duration is considered.

predictions of CO₂ saturation in wells M1 and M5. Significant uncertainties can also be seen in the predictions of pressure data at the monitoring well locations, especially during the injection period (first five years). Similar observations can be found in the predictions of CO₂ saturation and pressure data in wells M2, M3 and M4, which are not shown here.

To reduce the uncertainty in the predictions, monitoring data are collected at the monitoring wells after start of CO₂ injection. The monitoring data are assimilated into reservoir models after different monitoring durations, such as 1 and 3 years. Note that 1 and 3 year monitoring durations are monthly for the first year of injection and monthly for the first three years of injection, respectively. The longest monitoring duration considered in this study is 10 years which include 5-year post-injection period. After each data assimilation iteration the updated reservoir models are used to perform future predictions and quantify uncertainties. Fig. 8 shows the comparison between CO₂ saturation at monitoring wells predicted with pre-injection models (cyan curves) and updated models (blue curves) for all 100 realizations. The figure shows results for different monitoring durations. It can be observed from Fig. 8 that the variability in the predictions of CO₂ saturation is reduced by assimilating monitoring data after different monitoring durations (i.e., 1, 5 and 7 years) and the reduction in variability increases with increased monitoring data assimilation. Similar observations can be found in the predictions of pressure data based on posterior models (see Fig. 9), but most of the reduction in variability in the pressure data takes place after assimilation of first year of monitoring data.

To quantitatively evaluate the uncertainty reduction in the predictions of CO₂ saturation and pressure at the end of the project (15 years), we compute the uncertainty of CO₂ saturation and pressure ($P(J|d_{obs})$ in Eq. (6)) at the end of 15 years considering different monitoring durations, i.e., 1, 3, 5, 7 and 10 years. The computed uncertainties in CO₂ saturation and pressure over the 10 years monitoring duration are shown in Fig. 10. The objective of our investigation is to assess how monitoring duration affects the uncertainties in the predictions of CO₂ saturation and pressure at the end of 15 years. It can be seen from Fig. 10(a) that most of the uncertainties in CO₂ saturation at the monitoring wells M1, M2 and M5, respectively, are reduced after assimilating monitoring data after the first 5, 3 and 7 years, respectively. There is no uncertainty in CO₂ saturation at M3 (the injector) and M4 at the end of 15 years according to the definition of uncertainty given in Eq. (5); see Fig. 11. From Fig. 10(b), we can see that most of the uncertainty in pressure at the end of 15 years is reduced after assimilating one year of monitoring data. However, the uncertainty reduction in the

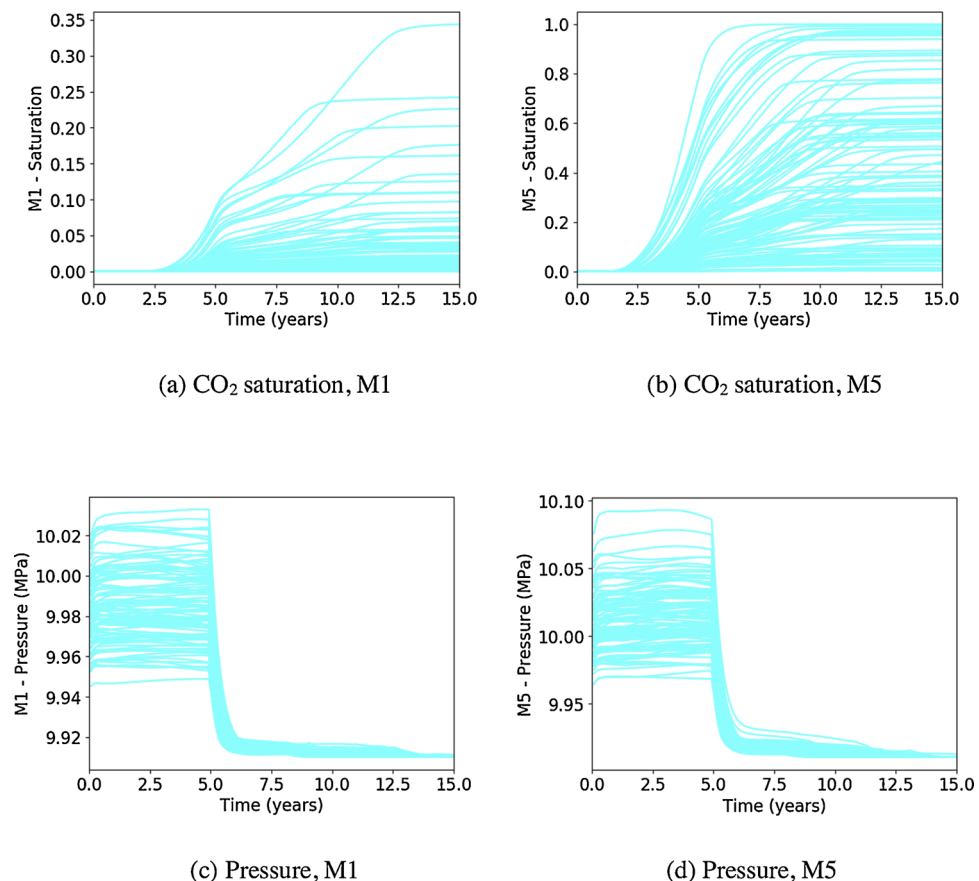


Fig. 7. The predictions (forecasts) of CO₂ saturation and pressure based on prior reservoir models at monitoring wells M1 and M5.

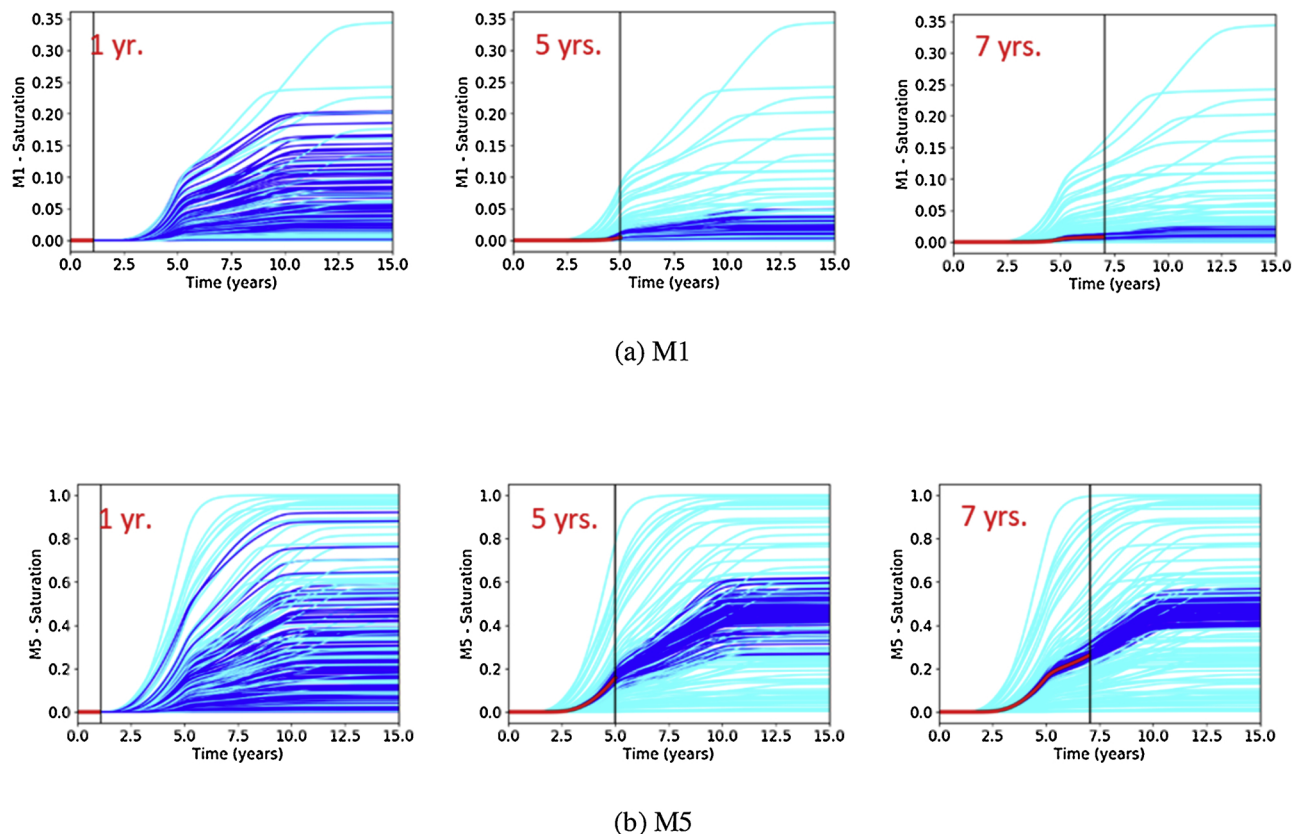


Fig. 8. Assimilating CO₂ saturation measurements collected within different monitoring durations (1, 3 and 7 years) at wells M1 and M5, and predictions of CO₂ saturation for the remaining years. Red lines represent the monitoring data generated by the ground truth model. Cyan lines represent the data from a priori models and blue lines represent the data from a posteriori models.

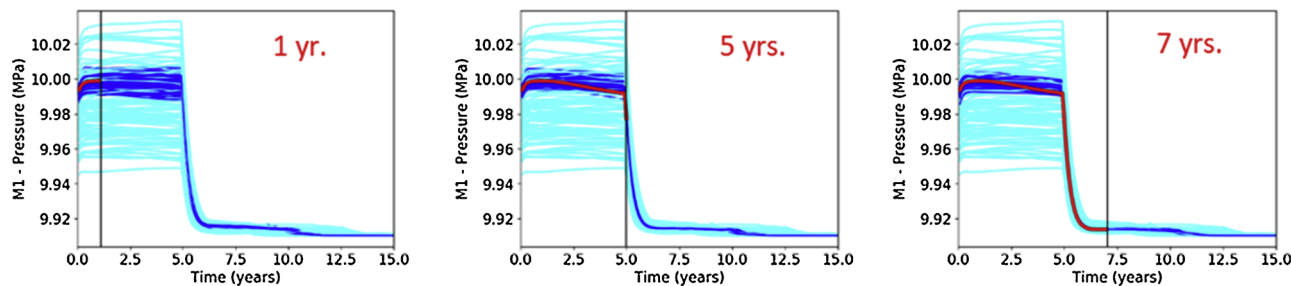
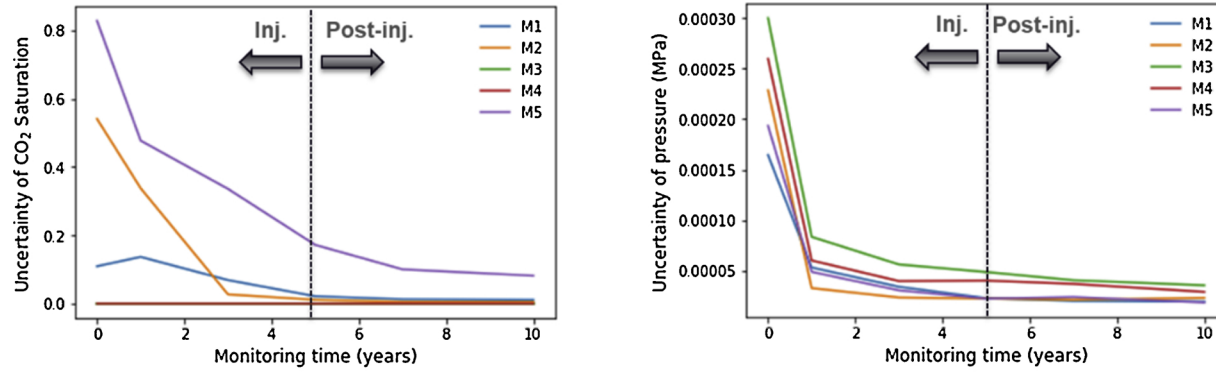


Fig. 9. Assimilating pressure measurements collected within different monitoring durations (1 year, 3 years and 7 years) at well M1, and predictions of pressure for the remaining years.



(a) Uncertainty of CO_2 saturation

(b) Uncertainty of pressure

Fig. 10. Uncertainty of CO_2 saturation and pressure over monitoring durations.

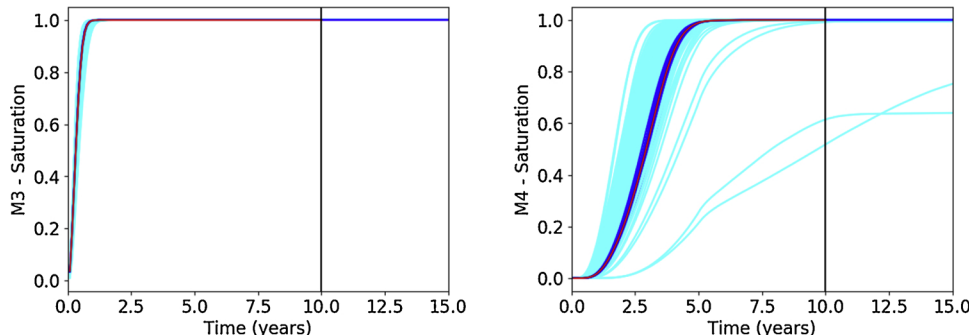


Fig. 11. History matching 10 years' CO_2 saturation data and prediction for the remaining 5 years at monitoring wells M3 and M4. Red lines represent the monitoring data generated by the ground truth model. Cyan lines represent the data from a priori models and blue lines represent the data from a posterior models.

prediction of pressure is not as significant as for CO_2 saturation due to the fact that the variability in the pressure change is small once the CO_2 injection stops (see blue lines after year 5 in Fig. 9 as an example).

The first example was used to demonstrate the effectiveness of the ES-MDA-GEO algorithm for assimilating monitoring data to refine reservoir models. In addition, the uncertainty reduction in the predictions of CO_2 saturation and pressure over different monitoring durations has been visualized. Next, we will demonstrate the proposed workflow for reducing uncertainty through monitoring data assimilation using data for a field site.

4. Example 2: Rock Springs Uplift site

4.1. Site description

Rock Springs Uplift (RSU), which is located in Southwestern Wyoming, has been identified as a potential site for CO_2 storage by the

Wyoming State Geological Survey (Surdam and Jiao, 2007). Fig. 12 is a stylized cross section of the RSU and adjacent basins. Our study uses the Lower Madison formation, one of the formations identified by Wyoming Geological Survey as potential CO_2 storage reservoirs. The average thickness of the Lower Madison formation in our model domain is 94 m. Note only part of this formation is used as the target area for the numerical simulation of CO_2 injection in this study. The distances from the RSU #1 to four boundaries (from east to north) of the target area are 3283 m, 2948 m, 2747 m and 3082 m, respectively.

The top image in Fig. 13 displays the computational mesh used in the reservoir simulation model. The computational mesh has approximate horizontal extents of 6.03 km by 6.03 km and from 2.8 km to 4.3 km below the ground surface. The bottom image in Fig. 13 displays the side view of the target reservoir, the Lower Madison formation. Pressure within the model is initialized using a hydrostatic pressure gradient with atmospheric pressure at the ground surface. This produces an initial pressure at the bottom of the CO_2 injection well of 37

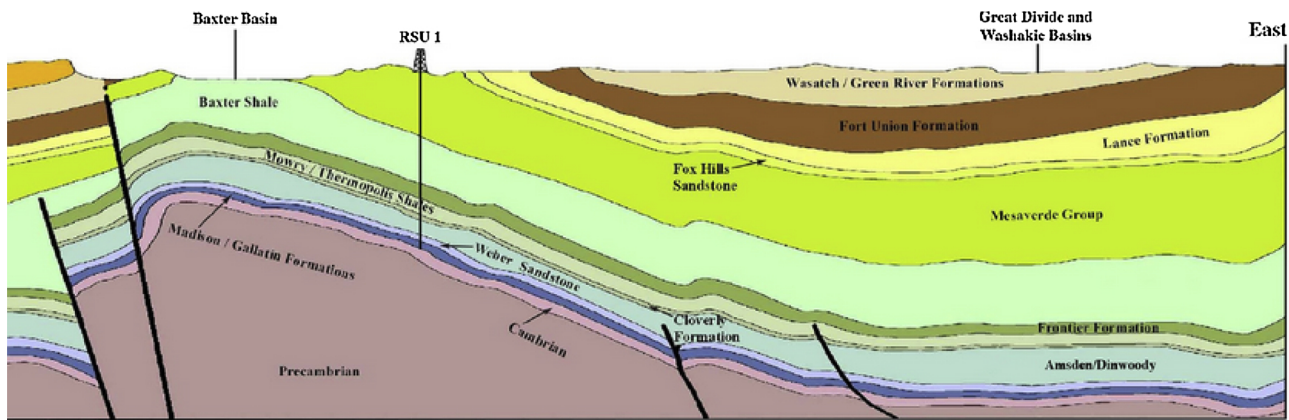


Fig. 12. Stylized geologic cross section through study site and adjacent basins. Madison formation is denoted by the blue stripe. Black lines at the left-hand side represent faults. (Surdam and Jiao (2007)).

MPa. Temperature within the model is initialized based on a geothermal gradient of $0.0255\text{ }^{\circ}\text{C/m}$ and an average surface temperature of $4.4\text{ }^{\circ}\text{C}$.

At RSU site only one exploratory well (RSU #1) has been drilled to the depth of the Lower Madison formation and has been used to collect multiple characterization data. The characterization data has been used to generate a geologic model for the site including, a spatial distribution of permeability for the Lower Madison formation (Surdam and Jiao, 2007). We assume this geologic model as the “ground truth” for the RSU site. We assume that in addition to the RSU #1 four more characterization wells are drilled to collect characterization data about the target storage reservoir prior to injection, and these wells later will be used as monitoring wells during the injection phase. The locations of these five characterization wells (M1 through M5) are shown in Fig. 14. RSU #1 is referred to as M3 in the later presentation. The upper right corner (solid blue region) in Fig. 14 is considered separated from the rest of the domain by a non-transmissive fault which exists within the RSU study domain. Since the true permeabilities for the four potential exploratory wells are unknown, we obtain these values from the synthetic “ground truth” model for the Lower Madison formation. The permeabilities in the Lower Madison formation at the locations of the five characterization wells (M1 through M5) are 14.98, 15.77, 10.49, 8.40 and $4.55\text{ }mD$, respectively. We assume no permeability variability in the vertical direction. In addition to the five characterization wells, we also assume three legacy wells, which are plugged and abandoned, exist at the site. These legacy wells are, denoted as N1, N2 and N3 on Fig. 14 (Note that, wells M1, M2, M4, M5, N1, N2 & N3 are hypothetical and assumed to exist only for this study).

We assume CO_2 is injected through well M3 at a rate of 1 MM tons/year (31.7 kg/s) over a duration of 10 years which is followed by a 50 years post-injection site care period. Similar to the previous example, we assume that the types of monitoring data collected from the field are pressure and CO_2 saturation. The frequency of the data acquisition program is once per month, which results in 12 measurements per year for both pressure and CO_2 saturation. These monitoring data are iteratively assimilated into the reservoir models to quantify uncertainty reduction in the predictions including various risk metrics. As in example 1, there is no GCS operation taking place at the RSU site and no actual monitoring data available for the site. We generate the monitoring data by performing a forward simulation based on the “ground truth” model.

4.2. Results and analysis

4.2.1. Permeability fields based on geostatistical conditional simulation

Based on the permeabilities obtained from the five exploratory wells, we compute the mean and variance of the permeabilities. The correlation length for the isotropic permeability distribution is assumed

to be 670 m (corresponding to the width of 10 cells of our computational mesh). With the mean and variance of the permeability distribution and the assumed correlation length, conditional simulation is conducted to generate 100 permeability fields for the Lower Madison formation using GSLIB software. The 100 permeability fields will be used to construct 100 prior models (pre-injection) of spatial permeability heterogeneity in this study. Note that other reservoir properties, such as porosity, can also be included in the conditional simulation, but only reservoir permeability is considered here, and other reservoir properties such as porosity distribution has been directly used from the ground truth model. Three examples of the permeability realizations generated using geostatistical conditional simulations are shown in Fig. 15. The permeabilities at the five monitoring (exploratory) wells are honored during conditional simulation, i.e., the permeability values at these five wells are pre-designated during the conditional simulation. Comparison of the permeability distribution of each realization generated from conditional simulation with the “ground truth” shows that the generated distributions are significantly different from the permeability field for the “ground truth” model (see Fig. 14), indicating large uncertainty in the generated prior models based on conditional simulation using the limited information available prior to injection.

4.2.2. Model improvement/refinement

In the earlier example, we have demonstrated how site-specific uncertainty can be reduced by assimilating monitoring data collected during GCS operations to update prior models. Fig. 16 shows the permeability distributions for the prior model and updated models based on 3- and 10-year monitoring durations for one of the 100 permeability realizations generated using conditional simulations. It can be seen that after the monitoring data assimilation is conducted, the permeability field is significantly updated (recovered). We can also see that the permeability field based on assimilating 10 years of monitoring data is much closer to the ground truth model than the prior model. The entire model improvement/refinement over monitoring is quantified in Fig. 17. It is important to note that the extent of model improvement is dependent on the number of monitoring wells (refer to Fig. 6).

Here, we take the case with 3-year monitoring duration as an example to show the computational cost for the data assimilation process using ES-MDA-GEO. The computational cost for the whole process includes three parts: the time for the forward simulation runs based on the prior models, the time for the simulation runs in the data assimilation process, and the time for the forward simulation runs based on posterior (updated) models. Note that the forward simulations based on the prior models only need to be executed one time. In other words, if the forward simulations based on the prior models have been executed in the case with 3-year monitoring duration, then it is no longer required to execute the forward simulation runs based on prior models

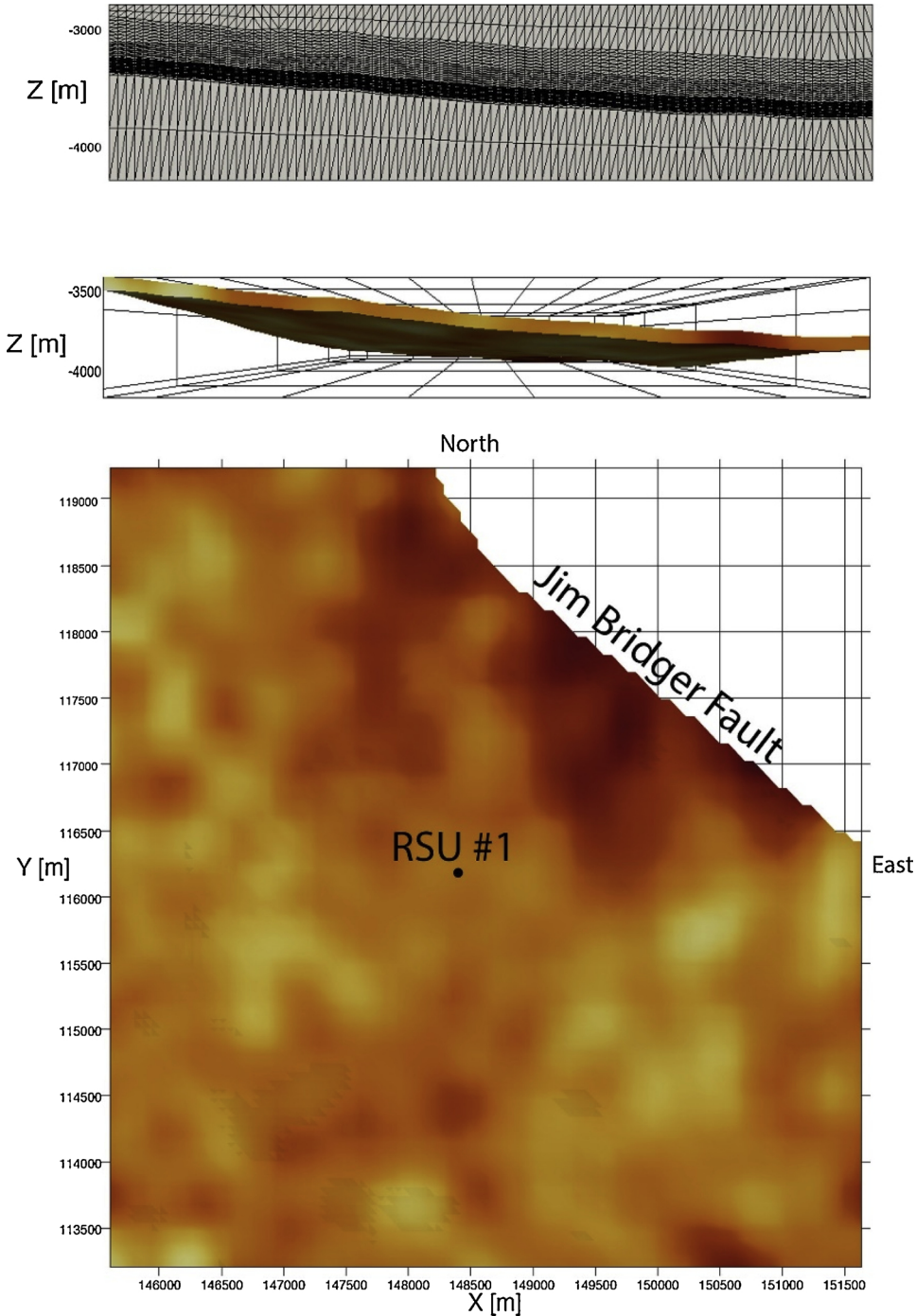


Fig. 13. A mesh side view is shown in the top image. Side and map views of Lower Madison is shown in the middle and bottom images. ([Harp et al. \(2017\)](#)).

again in the case with 10-year monitoring duration. For the simulation of 3-year monitoring duration in the data assimilation process, it took about 0.7 h for each simulation run using FEHM simulator. For the forward simulation of 60-year injection and post-injection period based on the prior models or the posterior models, each simulation run took about 6.7 h. If all the required simulations are executed sequentially, it took about $6.7 \times 100 + 0.7 \times 100 \times 4 + 6.7 \times 100 = 1620$ hours. The number ‘100’ denotes the ensemble size (i.e., the number of model realizations); ‘4’ denotes the number of data assimilation steps (i.e., N_a in the pseudo-code). Due to the independent property of each ensemble for the ensemble-based method (i.e., ES-MDA-GEO), all the required simulations in each data assimilation step and all the simulations based on prior and posterior models can be executed in parallel. Based on our

computational resources, we have 50 simulations executed in parallel. Thus, the actual time for the data assimilation process with 3-year monitoring duration is $1620/50 = 32.4$ hours. Note that we can have at most 100 simulations executed concurrently since the ensemble size is 100, so the minimum time cost for this field-scale case with 3-year monitoring duration is $1620/100 = 16.2$ hours.

4.2.3. Uncertainty reduction analysis of CO_2 saturation and pressure at monitoring wells

In the uncertainty reduction analysis, uncertainty reduction in different predicted metrics including, the predictions of CO_2 saturation and pressure at well locations, CO_2 saturation/pressure plume area/mobility/spreading are computed for different monitoring durations (1,

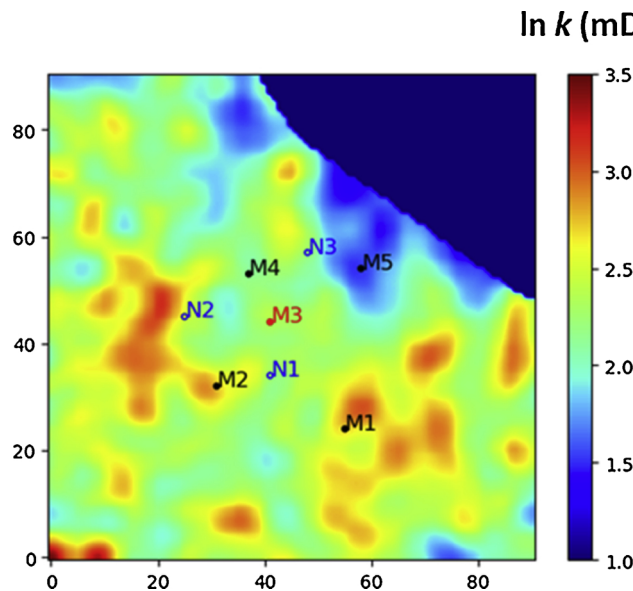


Fig. 14. Horizontal log-permeability distribution for the “ground truth” model. M1 through M5 are the locations for the five exploratory wells. N1, N2 and N3 are the locations for three legacy wells. The upper right corner (solid blue region) is considered separated from the rest of the domain by a non-transmissive fault.

3, 5, 10, 15 and 20 years). First, the uncertainty reductions in the predictions of CO₂ saturation and pressure at monitoring wells are analyzed. Fig. 18 shows the history matches and predictions of pressure and CO₂ saturation data at three monitoring well locations (M2, M3 & M5) after assimilating 3-year monitoring data. Note that the total CO₂ injection period is 10 years, and the post-injection duration is 50 years. We can see from Fig. 18 that significant uncertainty exists in the pressure data (see cyan lines) which are computed from the prior models (permeability realizations) in the first 10 years. A dramatic pressure decrease is observed after 10 years due to the fact that CO₂ injection ceases. From Fig. 18, it can also be seen that the pressure and CO₂ saturation data in the first 3 years are well matched. The uncertainty in the predictions of the pressure and CO₂ saturation data computed from posterior models (see blue lines) are much smaller than those computed from prior models (see cyan lines) after 3 years, especially for pressure data from year 3 to year 10. Due to the fact that the CO₂ saturation in injection well (M3) is equal to 1, thus no uncertainty in CO₂ saturation measurements is observed in the injection well; see Fig. 18(e).

The uncertainties in the predictions of CO₂ saturation and pressure at each monitoring well at the end of the project (60 years) for different monitoring durations are shown in Fig. 19. The purpose of this investigation is to show how longer monitoring durations reduce the uncertainties in the predictions of CO₂ saturation and pressure at the end of 60 years. As can be seen from Fig. 19(a), very little uncertainty exists in the predictions of CO₂ saturation at the end of 60 years at the locations of monitoring wells M2, M3 and M4 (the saturations at these wells are equal to 1; see Fig. 18(d) and (e) as examples), and a small amount of uncertainty remains in prediction of CO₂ saturation at wells M1 and M5 (see Fig. 18(f) for M5). While there is not much uncertainty to reduce in the predictions of CO₂ saturations at the monitoring well locations at the end of 60 years by assimilating monitoring data, it is critical to increase confidence in model predictions. From Fig. 19(b), we can see that most of the uncertainty in pressure data at all the monitoring well locations at the end of 60 years is reduced within the first 10 years. However, the maximum uncertainty reduction (about 0.04 MPa) is still not significant.

4.2.4. Uncertainty reduction analysis of CO₂ saturation and pressure at legacy wells

In the above analysis, we have analyzed the uncertainty reduction in CO₂ saturation and pressure at the monitoring well locations. For overall risk assessment it is important to effectively predict saturation and pressure at legacy wells (N1, N2 and N3 in Fig. 14) especially the ones which are plugged and abandoned. Next, we will investigate how the uncertainties in the predictions of CO₂ saturation and pressure at the legacy wells change with assimilation of monitoring data. We predict pressure and saturation at different times at legacy well locations by running forward simulations using the reservoir models that are iteratively updated through monitoring data assimilation.

Fig. 20 shows the predictions of pressure and CO₂ saturation at the legacy well locations over 60 year duration. The cyan lines correspond to the calculation based on the prior (pre-injection) models, while the blue lines correspond to the posterior models based on the 3-year monitoring duration. The red line corresponds to the calculation based on the ground truth model, and it is used for comparison of performance. As can be seen, the uncertainty in the (see blue lines in Fig. 20(a), (b) and (c)) is significantly smaller than that based on the prior models (see cyan lines in Fig. 20(a), (b) and (c)). However, the uncertainty reduction in CO₂ saturation is not as significant as that in the pressure data. This is due to the fact that the pressure changes travel much farther in the reservoir compared to saturation. For example, it can be seen that the CO₂ saturation plume does not reach at the monitoring wells M1, M2 and M5 at the end of year 3. Thus, there is little information available from CO₂ saturation measurements at these

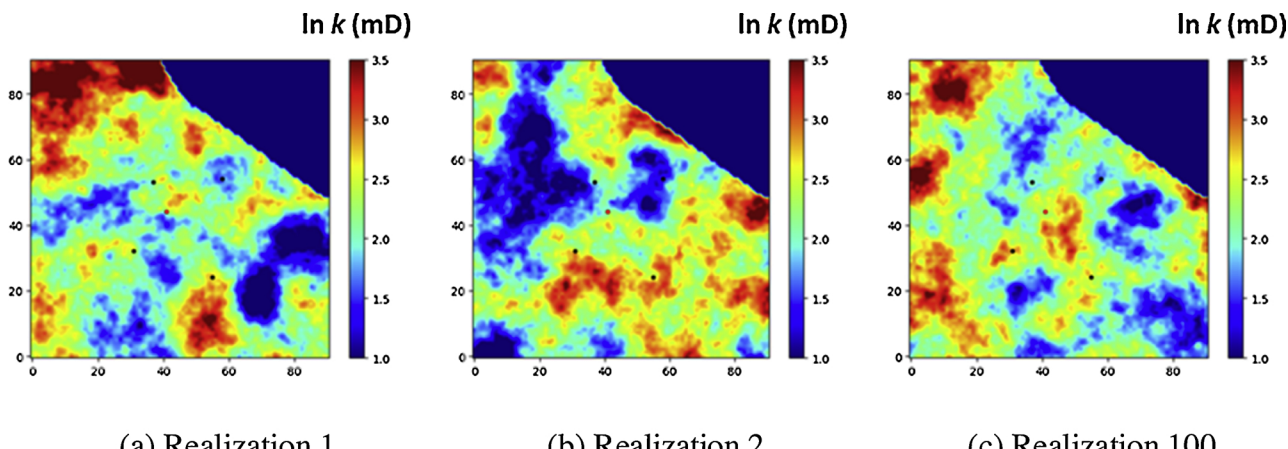


Fig. 15. Three realizations for permeability fields of the Lower Madison based on conditional simulation. Five black dots including one red dot in the figure denote the locations for the five exploratory wells respectively.

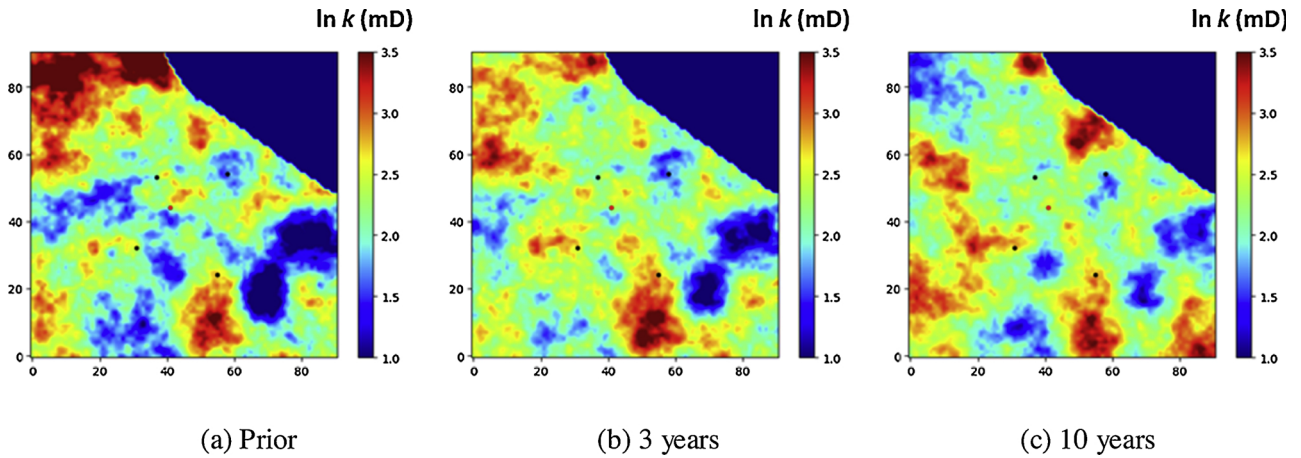


Fig. 16. Model improvement over monitoring duration, realization 1, example 2.

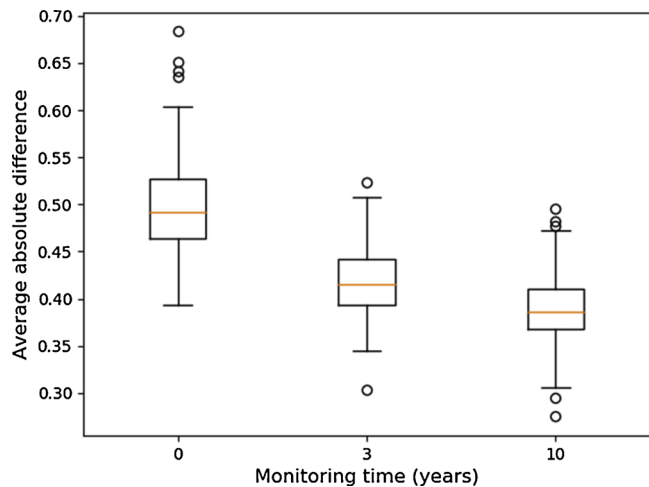


Fig. 17. Boxplot of average absolute difference between calibrated models and the ground truth model over monitoring duration, example 2. Circles in the plot are the outliers; five horizontal lines from bottom to top in each boxplot, respectively, represent the minimum, the 1st quartile, the median, the 3rd quartile and the maximum of a distribution.

locations for updating the reservoir models. Though no CO₂ breakthrough is also a ‘0’ data point and it needs to be matched by the models, this doesn’t mean that the “0” data points provide significant value for model updating. However, as the monitoring duration increases from 3 to 10 years, movement of CO₂ plume over increased duration does lead to observable changes at monitoring well locations which can lead to reducing the uncertainty in the predictions of CO₂ saturation; see Fig. 21.

The uncertainties in the predictions of CO₂ saturation and pressure at each legacy well at the end of the project (60 years) after assimilating monitoring data for different durations are shown in Fig. 22. It can be observed from Fig. 22(a) that the uncertainty in the prediction of pressure decreases with the increase of monitoring duration for the three legacy wells. Most of the uncertainties in the prediction of pressure at legacy wells are reduced after assimilating the first 15 years of monitoring data. However, the maximum uncertainty reduction in the pressure is less than 0.04 MPa which even though is not significant by itself, it is significant when considering the initial amount of uncertainty in pressure. We can see from Fig. 22(b) that there is little to no uncertainty in the prediction of CO₂ saturation at the end of 60 years at the legacy well N1. This is because the location of N1 is very close to the injection well, the CO₂ saturation values calculated from the posterior models are very close or equal to 1 at the end of 60 years at N1 (see

Fig. 21(a)). The uncertainty in the prediction of CO₂ saturation at N3 is small, which can be easily explained by the saturation distribution at the end of 60 years; see the cyan lines at the end of 60 years in Fig. 21(c). This small uncertainty can be reduced by only assimilating 1 year of monitoring data. Significant reduction in the uncertainty in the prediction of CO₂ saturation at N2 is observed after assimilation of 10-year monitoring data. However, a small increase of the uncertainty in the prediction of CO₂ saturation at N2 is observed after assimilating 15-year monitoring data, which indicates that increased assimilation of monitoring data does not always lead to reduced uncertainty in quantities such as pressure/saturation at legacy wells that are not directly conditional to any history data. Theoretically, if a quantity is directly conditional to history data, then increased assimilation of monitoring data can help to reduce the uncertainty in predictions or forecasts of this particular quantity. However, if a quantity is not directly conditional to any history data (such as CO₂ saturation data at legacy well), one cannot always guarantee more uncertainty reduction in the predictions, and the observations from point properties such as CO₂ saturation at legacy wells and averaged properties such as CO₂ saturation plume area (which will be discussed later) have demonstrated this.

4.2.5. Uncertainty reduction analysis in plume stability metrics over monitoring duration

In addition to the changes in reservoir pressure and saturation, it is also important to take into consideration evolution of CO₂ saturation and pressure plumes and different metrics that capture plume evolution including plume area, mobility of plume centroids, and spreading of plumes. Harp et al. (2019) have developed different quantitative metrics to capture the plume evolution. Fig. 23 shows the change of the predictions of pressure and CO₂ saturation plume areas over monitoring durations (0 and 3 years). From Fig. 23(a), we can see that there is large uncertainty in the prediction of pressure plume area during the injection period (the first 10 years), while large uncertainty in the prediction of CO₂ saturation plume area occurs during the post-injection period. It can be observed from Fig. 23(b) that the uncertainties in the predictions of pressure plume area during the injection period and CO₂ saturation plume area during the post-injection period are significantly reduced after assimilating 3 years of monitoring data.

Fig. 24 shows the uncertainty in the prediction of CO₂ plume area at the end of 60 years for different monitoring durations. It can be observed that the uncertainty in the prediction of CO₂ saturation plume area decreases with increases in monitoring duration, but most of the uncertainty is reduced after assimilation 5 years of monitoring data. We also see slight increase in uncertainty after assimilating 20-year monitoring data, which can be explained by the same reason (i.e., increased assimilation of monitoring data does not always lead to reduced uncertainty in quantities that are not directly conditional to any history

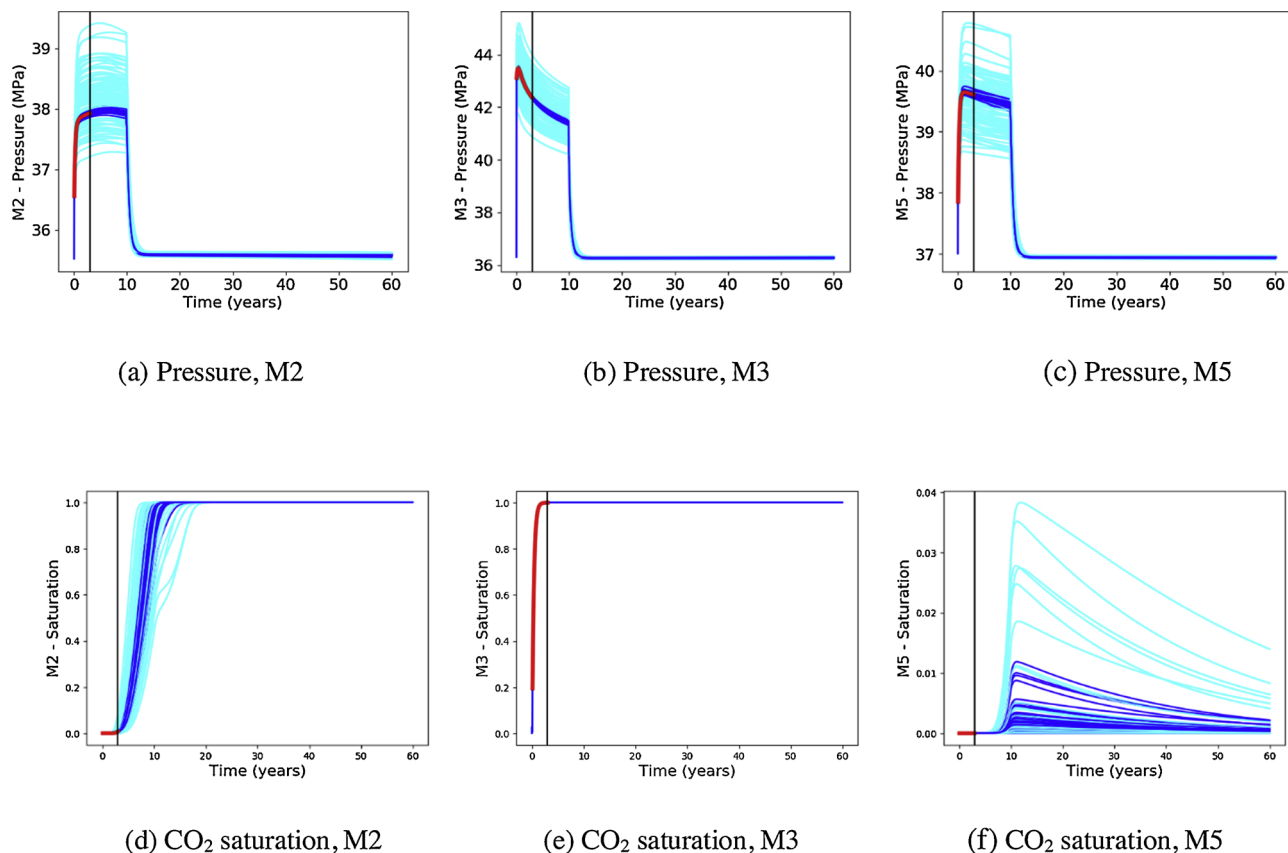


Fig. 18. Pressure and CO₂ saturation data matches for first 3 years (before vertical black line) and predictions of 57 years at monitoring wells. Red lines indicate the history data; cyan curves indicate the data computed from prior models and blue curves indicate the data computed from posterior models.

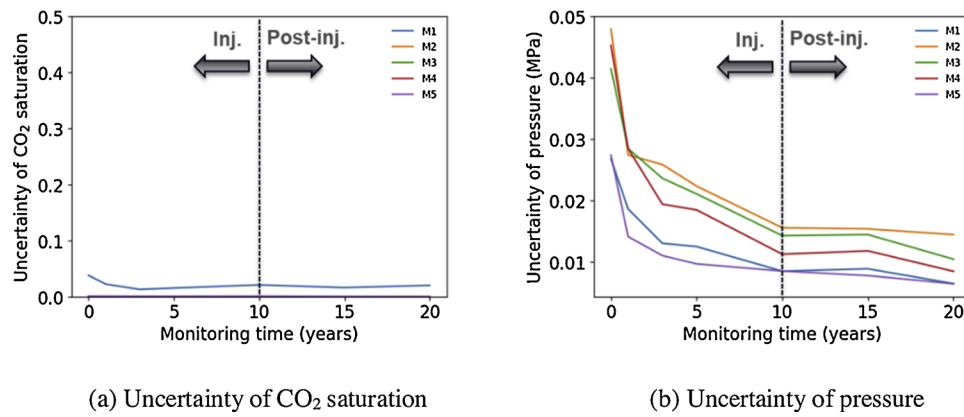


Fig. 19. Uncertainty of CO₂ saturation and pressure changing over monitoring time at monitoring wells.

data) for the observation of uncertainty increase in the prediction of CO₂ saturation at year 15 at the legacy well N2 (see Fig. 22(b)). The uncertainties in the predictions of pressure/CO₂ saturation plume mobility and spreading are also investigated. We see that the uncertainties in the predictions of these quantities are observed only in the early stage (within the first year) and assimilation of early stage monitoring data will help reduce this early stage uncertainty (figures are not shown in this paper).

It should be noted that the plume stability metrics discussed here reflect average quantities over an area or volume. While there can be large uncertainty in the permeability distribution, it does not lead to similar scale of uncertainty in averaged quantities. This is reflected in uncertainties computed for the different plume stability metrics mentioned above. Similarly, we do not observe similar effect of assimilating

monitoring data on reducing the uncertainty in plume stability metric as that in quantities such as pressure and saturation at well locations.

5. Conclusions

In this study, data assimilation and uncertainty reduction analysis in geologic CO₂ sequestration have been performed. Geostatistical conditional simulations were used to incorporate the data collected from characterization wells into the generation of prior (pre-injection) site geologic and reservoir models. To assimilate the data collected from monitoring operations and generate posterior models conditional to monitoring data, a recently developed data assimilation approach, ESMDA-GEO, has been applied. Based on the prior and posterior (updated) models, the uncertainty reductions in predictions of different

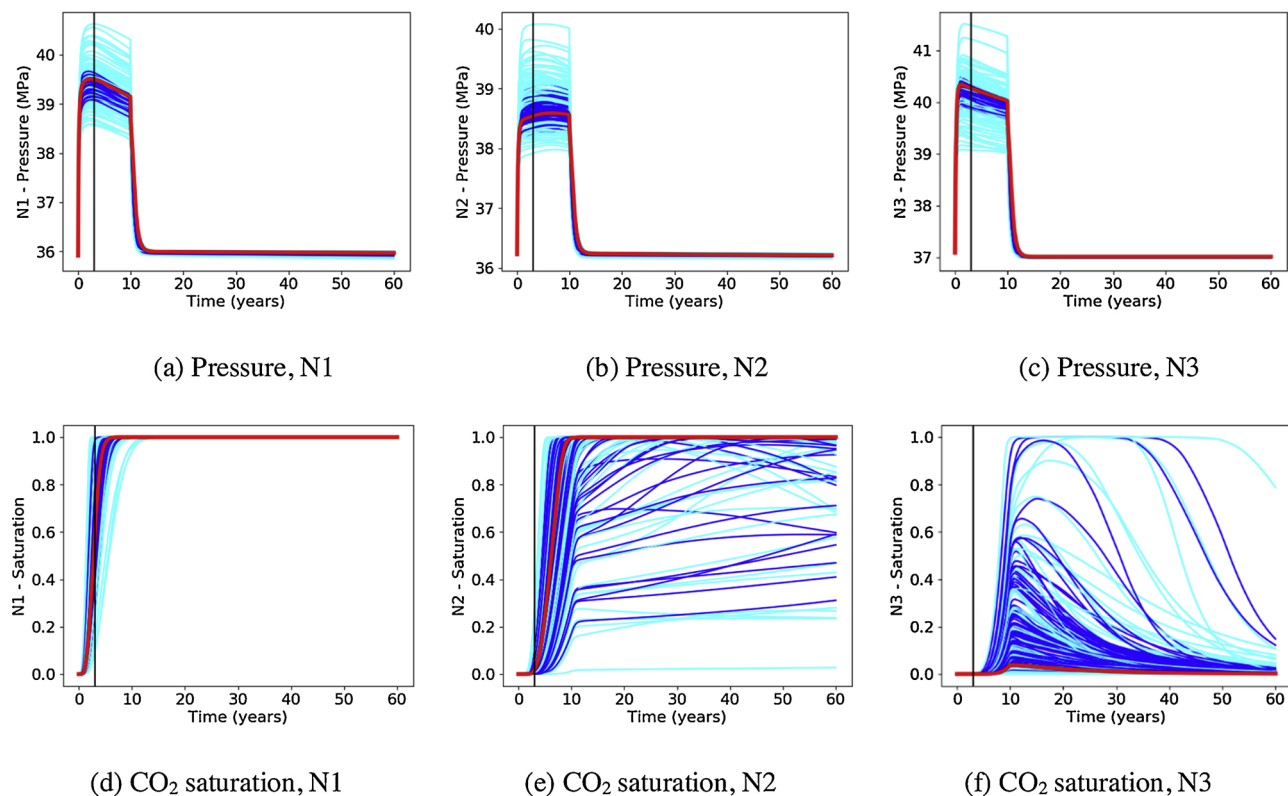


Fig. 20. Prediction of pressure and CO₂ saturation in 60 years at the legacy well based on a 3-year monitoring duration. The cyan lines correspond to the prior models; the blue lines correspond to the posterior models; the red line corresponds to the ground truth model.

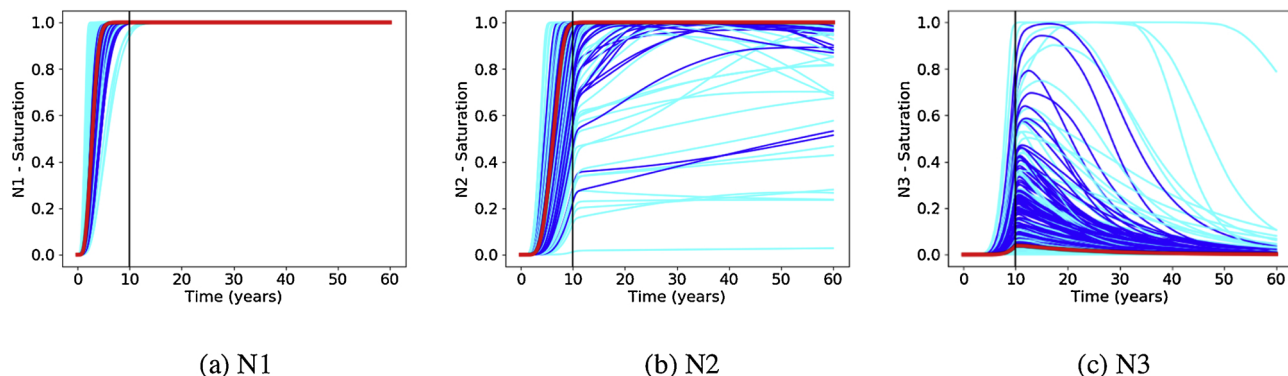


Fig. 21. Prediction of CO₂ saturation in 60 years at the legacy well based on a 10-year monitoring duration. The cyan lines correspond to the prior models; the blue lines correspond to the posterior models; the red line corresponds to the ground truth model.

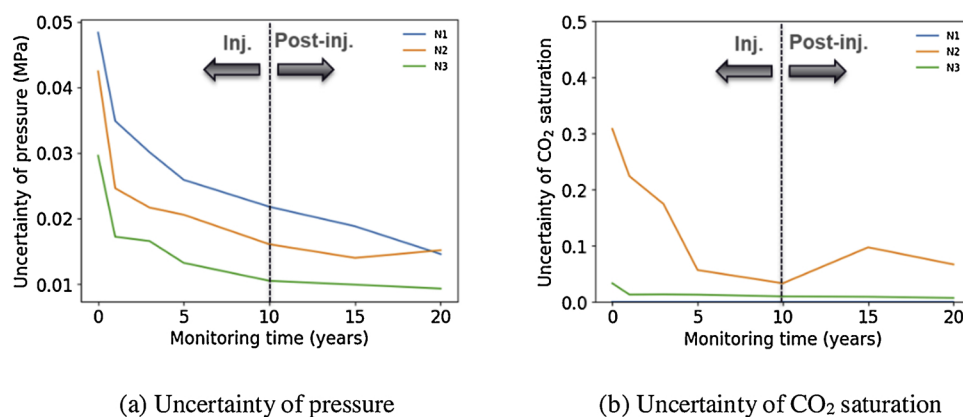


Fig. 22. Uncertainty of CO₂ saturation and pressure as a function of monitoring duration at legacy wells.

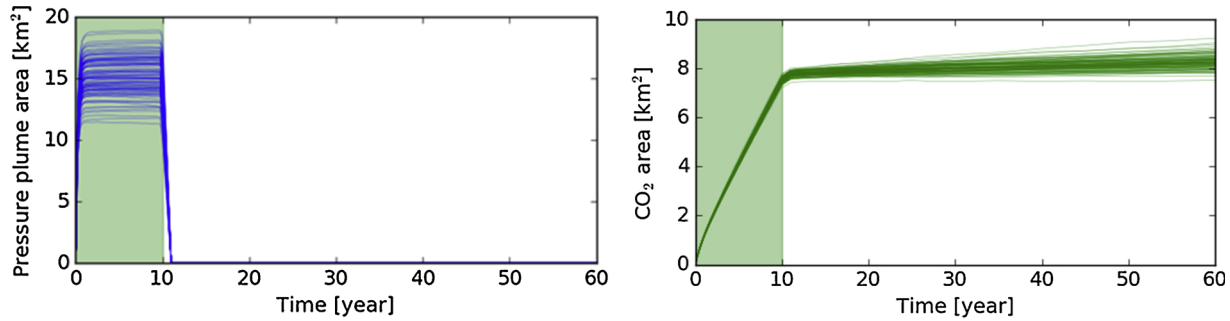
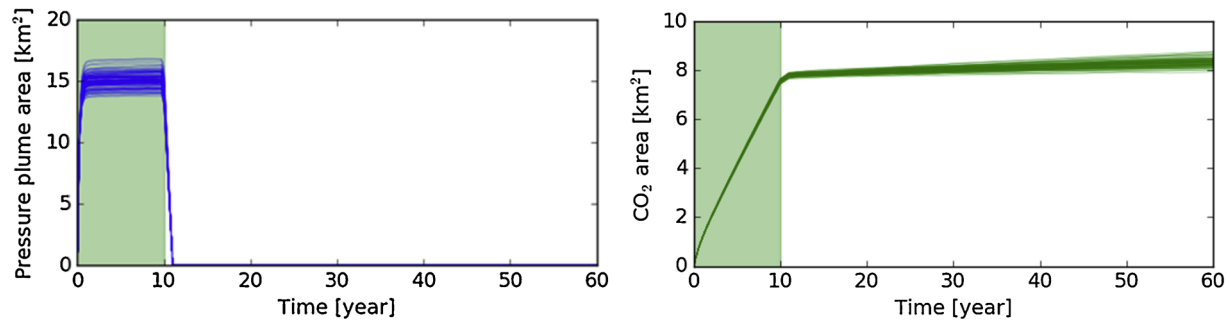
(a) Pressure plume area (left) and CO₂ saturation plume area (right), prior models(b) Pressure plume area (left) and CO₂ saturation plume area (right), 3 years monitoring data

Fig. 23. The change of the predictions of pressure and CO₂ saturation plume areas over monitoring durations. In these figures, blue lines stand for the pressure plume area over time; green lines represent the CO₂ saturation plume area over time; green areas indicate the CO₂ injection period.

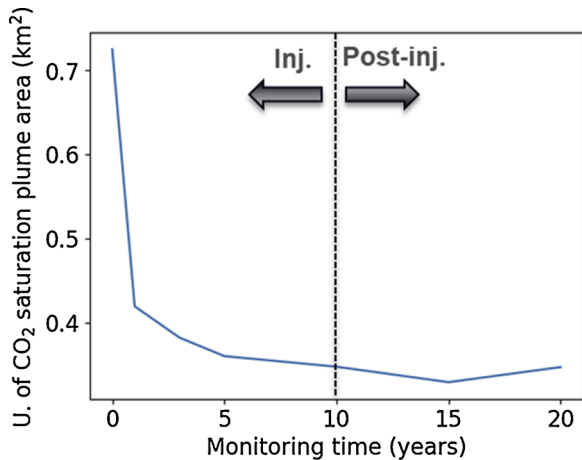


Fig. 24. Uncertainty in the prediction of CO₂ saturation plume area at the end of the project as a function of monitoring duration.

quantities such as CO₂ saturation and pressure, plume areas, plume centroid velocity and plume spreading metrics have been computed after assimilation of monitoring data to investigate how assimilating monitoring data over different monitoring durations affects the uncertainty reduction in predicted quantities. The results have been demonstrated with two examples: a synthetic example and an example based on data collected at the Rock Springs Uplift site in Wyoming. The following conclusions can be drawn from this study:

- The ensemble-based algorithm, ES-MDA-GEO, can be used to effectively assimilate the data collected from the monitoring operation of CO₂ storage. Due to the independent property of each ensemble for the ensemble-based method, all the required forward simulations

in each data assimilation step can be executed in parallel (i.e., concurrently), thus the use of ES-MDA-GEO is also efficient.

- The uncertainty reduction analysis approach can be applied to quantify the amount of uncertainty reduction in different quantities including different risk metrics, which can ultimately guide the determination of what is the effective monitoring duration to reduce the uncertainties in predictions of different metrics including long-term risks.
- The reservoir models can be significantly improved/refined with repeated assimilation of monitoring data, but the extent of model improvement is dependent on the number of monitoring wells.
- Assimilation of monitoring data can significantly reduce the uncertainties in predictions including during the post-injection period. The amount of reduction depends on the predicted quantities (e.g., pressure/CO₂ saturation) and locations (e.g., M1, M2..., M5 and N1, N2, N3 at RSU site) at which predictions are made.
- More data acquired from monitoring wells cannot always guarantee more uncertainty reduction in the prediction of quantities (for example, point properties such as CO₂ saturation at legacy wells or averaged properties such as CO₂ saturation plume area) that are not directly conditional to any history data.

It is important to note that in this study we only considered the quantities such as CO₂ saturations, pressures and their respective plume metrics. The same approach can be applied to assess the effectiveness of monitoring and monitoring duration to reduce uncertainty in risk metrics such as CO₂/brine leakage rates through legacy wells and groundwater aquifer impact (TDS/pH plume size) of CO₂/brine leaks and improve long-term leakage risk predictions. Quantification of uncertainty reduction in wellbore leakage rates and groundwater aquifer impact in legacy wells requires the use of quantitative approaches such as integrated assessment model (IAM) which couples the reservoir model, wellbore model and aquifer model, which will be the focus of

future research.

Declaration of Competing Interest

The authors declare that they have no known competing financial interests or personal relationships that could have appeared to influence the work reported in this paper.

Acknowledgements

This work was supported by the US Department of Energy through the Los Alamos National Laboratory. Los Alamos National Laboratory is operated by Triad National Security, LLC, for the National Nuclear Security Administration of U.S. Department of Energy (Contract No. 89233218CNA000001). This work was completed as part of the National Risk Assessment Partnership (NRAP) project. Support for this project came from the U.S. Department of Energy's (DOE) Office of Fossil Energy's Coal Research program. The authors wish to acknowledge Traci Rodosta and Mary K. Underwood (NETL Strategic Center for Coal) and Mark Ackiewicz and Darin Damiani (DOE Office of Fossil Energy) for programmatic guidance, direction, and support.

References

- Aanonsen, S.I., Nævdal, G., Oliver, D.S., Reynolds, A.C., Vallès, B., 2009. The ensemble Kalman filter in reservoir engineering—A review. *SPE J.* 14 (03), 393–412.
- Benson, S.M., Myer, L., 2003. Monitoring to ensure safe and effective geologic sequestration of carbon dioxide. Workshop on Carbon Dioxide Capture and Storage.
- Chang, H., Zhang, D., Lu, Z., 2010. History matching of facies distribution with the EnKF and level set parameterization. *J. Comput. Phys.* 229 (20), 8011–8030.
- Chen, B., Harp, D.R., Lin, Y., Keating, E.H., Pawar, R.J., 2018. Geologic CO₂ sequestration monitoring design: a machine learning and uncertainty quantification based approach. *Appl. Energy* 225, 332–345.
- Chen, B., Pawar, R.J., 2019. Characterization of CO₂ storage and enhanced oil recovery in residual oil zones. *Energy* 183, 291–304.
- Chen, Y., Oliver, D.S., 2010. Cross-covariances and localization for EnKF in multiphase flow data assimilation. *Comput. Geosci.* 14 (4), 579–601.
- Condor, J., Unatrakarn, D., Wilson, M., Asghari, K., 2011. A comparative analysis of risk assessment methodologies for the geologic storage of carbon dioxide. *Energy Procedia* 4, 4036–4043.
- Cui, G., Wang, Y., Rui, Z., Chen, B., Ren, S., Zhang, L., 2018. Assessing the combined influence of fluid-rock interactions on reservoir properties and injectivity during CO₂ storage in saline aquifers. *Energy* 155, 281–296.
- Dai, Z., Stauffer, P.H., Carey, J.W., Middleton, R.S., Lu, Z., Jacobs, J.F., Hnottavange-Telleen, K., Spangler, L.H., 2014. Pre-site characterization risk analysis for commercial-scale carbon sequestration. *Environ. Sci. Technol.* 48 (7), 3908–3915.
- Dai, Z., Zhang, Y., Bielicki, J., Amooie, M.A., Zhang, M., Yang, C., Zou, Y., Ampomah, W., Xiao, T., Jia, W., Middleton, R., Zhang, W., Sun, Y., Moortgat, J., S. M.R., Stauffer, P., 2018. Heterogeneity-assisted carbon dioxide storage in marine sediments. *Appl. Energy* 225, 876–883.
- De Lary, L., Manceau, J.C., Loscheret, A., Rohmer, J., Bouc, O., Gravaud, I., Chiaberge, C., Willaume, P., Yalamas, T., 2015. Quantitative risk assessment in the early stages of a CO₂ geological storage project: implementation of a practical approach in an uncertain context. *Greenh. Gases Sci. Technol.* 5 (1), 50–63.
- Deutsch, C.V., Journel, A.G., 1998. GSLIB: Geostatistical Software Library and User's Guide. Oxford University Press.
- Emerick, A.A., Reynolds, A.C., 2013. Ensemble smoother with multiple data assimilation. *Comput. Geosci.* 55, 3–15.
- Evensen, G., 2009. Data Assimilation: the Ensemble Kalman Filter. Springer Science & Business Media.
- Evensen, G., 2018. Analysis of iterative ensemble smoothers for solving inverse problems. *Comput. Geosci.* 22 (3), 885–908.
- George, D., Kuprat, A., Carlson, N., Gable, C., 1999. LaGriT-Los Alamos Grid Toolbox.
- Harp, D.R., Onishi, T., Chu, S., Chen, B., Pawar, R.J., 2019. Development of quantitative metrics of plume migration at geologic CO₂ storage sites. *Greenh. Gases Sci. Technol.* 9, 687–702.
- Harp, D.R., Pawar, R., Carey, J.W., Gable, C.W., 2016. Reduced order models of transient CO₂ and brine leakage along abandoned wellbores from geologic carbon sequestration reservoirs. *Int. J. Greenh. Gas Control.* 45, 150–162.
- Harp, D.R., Stauffer, P.H., O'Malley, D., Jiao, Z., Egenolf, E.P., Miller, T.A., Martinez, D., Hunter, K.A., Middleton, R.S., Bielicki, J.M., 2017. Development of robust pressure management strategies for geologic CO₂ sequestration. *Int. J. Greenh. Gas Control.* 64, 43–59.
- Jia, W., McPherson, B., Pan, F., Dai, Z., Xiao, T., 2018. Uncertainty quantification of CO₂ storage using Bayesian model averaging and polynomial chaos expansion. *Int. J. Greenh. Gas Control.* 71, 104–115.
- Jin, L., Hawthorne, S., Sorensen, J., Pekot, L., Kurz, B., Smith, S., Heebink, L., Hergegen, V., Bosschart, N., Torres, J., Dalkhaa, C., Peterson, K., Gorecki, C., Steadman, E., Harju, J., 2017. Advancing CO₂ enhanced oil recovery and storage in unconventional oil play—Experimental studies on Bakken shales. *Appl. Energy* 208, 171–183.
- Kim, S., Min, B., Lee, K., Jeong, H., 2018. Integration of an iterative update of sparse geologic dictionaries with ES-MDA for history matching of channelized reservoirs. *Geofluids* 2018.
- Le, D.H., Emerick, A.A., Reynolds, A.C., 2016. An adaptive ensemble smoother with multiple data assimilation for assisted history matching. *SPE J.* 21 (2), 195–207.
- Le, D.H., Reynolds, A.C., 2014. Estimation of mutual information and conditional entropy for surveillance optimization. *SPE J.* 19 (04), 648–661.
- Li, Q., Liu, G., 2016. Risk Assessment of the Geological Storage of CO₂: a Review. *Geologic Carbon Sequestration*. Springer, pp. 249–284.
- Liu, M., Mostaghimi, P., 2017. Pore-scale modelling of CO₂ storage in fractured coal. *Int. J. Greenh. Gas Control.* 66, 246–253.
- Metz, B., 2005. Carbon Dioxide Capture and Storage: Special Report of the Intergovernmental Panel on Climate Change. Cambridge University Press.
- Michael, K., Golab, A., Shulakova, V., Ennis-King, J., Allinson, G., Sharma, S., 2010. Geological storage of CO₂ in saline aquifers—A review of the experience from existing storage operations. *Int. J. Greenh. Gas Control.* 4 (4), 659–667.
- Nicot, J.-P., Oldenburg, C.M., Houseworth, J.E., Choi, J.-W., 2013. Analysis of potential leakage pathways at the Cranfield, MS, USA, CO₂ sequestration site. *Int. J. Greenh. Gas Control.* 18, 388–400.
- Oladyshkin, S., Class, H., Nowak, W., 2013. Bayesian updating via bootstrap filtering combined with data-driven polynomial chaos expansions: methodology and application to history matching for carbon dioxide storage in geological formations. *Comput. Geosci.* 17 (4), 671–687.
- Onishi, T., Nguyen, M.C., Carey, J.W., Will, B., Zaluski, W., Bowen, D.W., Devault, B.C., Duguid, A., Zhou, Q., Fairweather, S.H., Spangler, L.H., Stauffer, P.H., 2019. Potential CO₂ and brine leakage through wellbore pathways for geologic CO₂ sequestration using the National Risk Assessment Partnership tools: application to the Big Sky Regional Partnership. *Int. J. Greenh. Gas Control.* 81, 44–65.
- Pawar, R., Bromhal, G.S., Chu, S., Dilmore, R.M., Oldenburg, C.M., Stauffer, P.H., Zhang, Y., Guthrie, G.D., 2016. The National Risk Assessment Partnership's integrated assessment model for carbon storage: a tool to support decision making amidst uncertainty. *Int. J. Greenh. Gas Control.* 52, 175–189.
- PetroWiki, 2012. Geostatistical Conditional Simulation.
- Rafiee, J., Reynolds, A.C., 2017. "Theoretical and efficient practical procedures for the generation of inflation factors for ES-MDA. *Inverse Probl.* 33, 115003.
- Ren, B., Duncan, I.J., 2019. Reservoir simulation of carbon storage associated with CO₂ EOR in residual oil zones, San Andres formation of West Texas, Permian Basin, USA. *Energy* 167, 391–401.
- Silva, V.L.S., Emerick, A.A., Couto, P., Alves, J.L.D., 2017. History matching and production optimization under uncertainties—application of closed-loop reservoir management. *J. Pet. Sci. Eng.* 157, 860–874.
- Sun, W., Durlofsky, L.J., 2019. Data-space approaches for uncertainty quantification of CO₂ plume location in geological carbon storage. *Adv. Water Resour.* 123, 234–255.
- Surdam, R.C., Jiao, Z., 2007. The Rock Springs Uplift: an Outstanding Geological CO₂ Sequestration Site in Southwest Wyoming. Wyoming State Geological Survey.
- Wilkin, R.T., DiGiulio, D.C., 2010. Geochemical impacts to groundwater from geologic carbon sequestration: controls on pH and inorganic carbon concentrations from reaction path and kinetic modeling. *Environ. Sci. Technol.* 44 (12), 4821–4827.
- Zhang, J., Wang, Z., Liu, S., Zhang, W., Yu, J., Sun, B., 2019a. Prediction of hydrate deposition in pipelines to improve gas transportation efficiency and safety. *Appl. Energy* 253, 113521.
- Zhang, K., Jia, N., Liu, L., 2019b. CO₂ storage in fractured nanopores underground: phase behaviour study. *Appl. Energy* 238, 911–928.
- Zhang, Y., Vouzis, P., Sahinidis, N.V., 2011. GPU simulations for risk assessment in CO₂ geologic sequestration. *Comput. Chem. Eng.* 35 (8), 1631–1644.
- Zyvoloski, G.A., Robinson, B.A., Dash, Z.V., Trease, L.L., 1997. User's Manual for the FEHM application-A Finite-element Heat-and Mass-transfer Code.